Influence of Arc Pressure on Weld Pool Geometry

A new model of a compound vortex is proposed as a possible mechanism to explain the deep surface depression encountered at currents over 300 amperes

BY M. L. LIN AND T. W. EAGAR

ABSTRACT. At currents over 300 amperes, the surface of the weld pool becomes markedly depressed and the assumption of a flat surface is no longer valid. In order to predict the weld pool geometry, the shape of the surface depression under the action of the arc pressure has been calculated.

At currents of 300 amperes, it is found that the arc pressure cannot account for either the depth or the shape of the experimentally observed surface depression. Instead, a new model of a compound vortex is proposed as a possible mechanism to explain the deep surface depression in this current range.

Introduction

A number of investigators have studied the magnitude of arc pressure in gas tungsten arcs (Refs. 1-6). Some attempts have been made to explain the formation of several weld defects such as humped beads, finger penetration and undercutting (Refs. 6,7,8) based on the assumption that the arc pressure depresses the surface of the weld pool. An analytical model was developed by Friedman (Ref. 9) to simulate the distortion of fully penetrated molten pools in thin plates under the action of arc pressure and gravitational forces.

In our own experiments, we have studied the influence of welding currents on the depth and shape of the surface depression (Ref. 10). Surprisingly, it was found that the surface depression depth is very small (less than 1 mm, *i.e.,* 0.04 in.) at currents up to 240 amperes (A), but the depth increases rapidly as the current is increased by 30 A—Fig. 1. This rapid change in surface depression depth is difficult to explain by the increase in arc pressure which scales parabolically with weld current (Ref. 11). Arc pressure also will not explain why one current value (*e.g.,* 260 A) can give either a depth of 1 mm (0.04 in.) or a depth of 5 mm (0.20 in.).

In order to evaluate whether arc forces of the magnitudes measured previously (Ref. 2) are capable of explaining the experimentally observed surface depression depths, an analytical model was developed. This model accounts for the balance of hydrostatic potential energy and surface energy with the work performed by the arc pressure displacing the liquid.

It will be seen that this model may be used to explain the experimental observations at low currents where surface depression is shallow; however, the results cannot explain the experimental evidence obtained at high currents where the depth is significant. As a result, the assumption that arc pressure significantly alters weld pool geometry is no longer considered to be valid. Instead, a simplified convection model is proposed which can, in principle, explain the very deep surface depression of the weld pool at high currents.

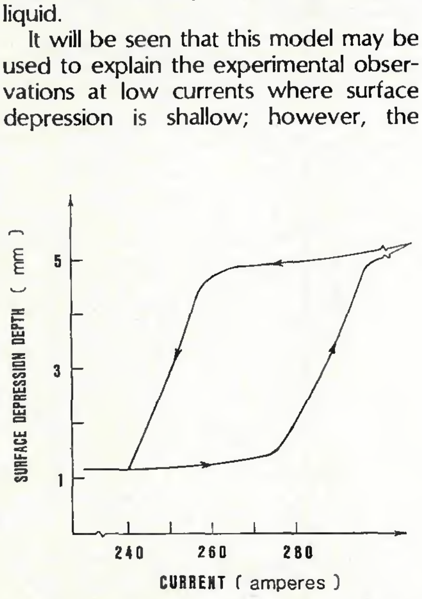

Fig. 1—Variation of surface depression depth with current, as observed experimentally. The arrows denote increasing and decreasing current and the fact that a hysteresis in surface depression exists as current is changed

Analytical Model

The surface depression will form a shape which minimizes the total energy; hence, calculus of variations may be used to calculate this shape under the action of arc pressure subject to the constraint that the volume of the weld pool is constant. In this model, it is assumed that there is no convection in the molten pool and that the weld is of the partial joint penetration type. In addition, for ease of analysis, cylindrical symmetry is assumed.

The energy to be minimized is the surface energy plus the potential energy of the liquid pool. Analytically, this takes the form

$$J = \int_0^R \sigma \cdot 2\pi r \left[1 + \left(\frac{dw}{dr}\right)^2 \right]^{1/2} dr + \int_0^R \rho g \cdot 2\pi r(h - w)\left(H - \frac{h + w}{2}\right) dr \qquad (1)$$

where the first integral on the right hand side of equation (1) is the interfacial energy between the gas and the liquid phase and the second integral is the potential energy of the liquid pool, with respect to a reference plane at h = H. The geometry of this system is shown in Fig. 2.

Equation (1) is subject to two constraints. First, constant liquid volume, which can be expressed as:

Based on a paper presented at the 65th Annual AWS Convention held in Dallas, Texas, during April 8-13, 1984.

M. L. LIN and T. W. EAGAR are associated with the Materials Processing Center, Massachusetts Institute of Technology, Cambridge, Massachusetts.

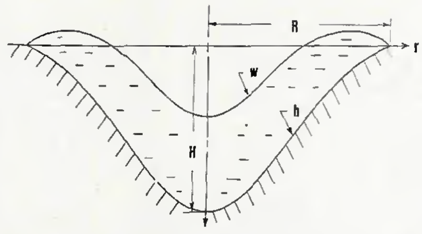

Fig. 2—Geometry of depressed weld pool showing the definitions of several parameters used in this model

$$\int_O^R G_1 dr = \int_O^R 2\pi r w dr = 0 \qquad (2)$$

where $G_1 = 2\pi r w$.

The second constraint requires that the work performed by the arc force be equal to the change of surface energy and potential energy of the liquid pool. However, the description of this constraint requires some discussion.

The first law of thermodynamics tells us that the energy of the system is conserved; however, the work performed by the arc force is not a state function but is path dependent. Consider the application of the arc pressure instantaneously. The volume of the liquid will be displaced by an amount ΔV and the work is $P\Delta V$; however, this work is not reversible.

The path of this form of work is given by ABC in Fig. 3 and the work is the area ABCD. If on the other hand, one considers that the pressure is increased slowly and incrementally, the volumetric displacement of the liquid might follow a path similar to AC in Fig. 3. The work done in this case is given by the area ACD. This would be the reversible work. If we assume that the volumetric displacement changes proportionally to the increased pressure, the reversible work is one-half of the irreversible work of path ABC. Depending on the path chosen, the efficiency of work may vary. Thus, another variable η is introduced to account for the efficiency of work conversion.

Accordingly, we may equate the work performed by the arc force to the change in surface energy and potential energy of the liquid pool by the following:

$$\int_O^R G_2 dr = \int_O^R G_3 dr + \int_O^R G_4 dr \qquad (3)$$

where $G_2 = \eta P_{arc} 2\pi r w$ and $\int_O^R G_2 dr$ is the fraction of work done by the arc force on the molten pool. The next term G_3 is given by:

$$G_3 = \sigma 2\pi r \left[1 + \left(\frac{dw}{dr}\right)^2 \right]^{1/2} - \sigma 2\pi r$$

where $\int_O^R G_3 dr$ is the difference between surface energy with surface depression and surface energy without surface depression of the molten pool, and finally

$$G_4 = \rho g 2\pi r (h - w)\left(H - \frac{h + w}{2}\right) - \rho g 2\pi r h \left(H - \frac{h}{2}\right) = \rho g 2\pi r \left(\frac{w^2}{2} - wH\right)$$

where $\int_O^R G_4 dr$ is the difference between potential energy with surface depression and potential energy without surface depression of the molten pool.

Using equation (2), J can be simplified as:

$$J = \int_O^R \sigma 2\pi r \left[1 + \left(\frac{dw}{dr}\right)^2 \right]^{1/2} dr + \int_O^R \rho g 2\pi r \left(Hh + \frac{w^2}{2} - \frac{h^2}{2}\right) dr$$

If we define

$$F = \sigma 2\pi r \left[1 + \left(\frac{dw}{dr}\right)^2 \right]^{1/2} + \rho g 2\pi r \left(Hh + \frac{w^2}{2} - \frac{h^2}{2}\right)$$

then $J = \int_O^R F dr$

Again using equation (2), equation (3) can be reduced to

$$\int_O^R G_2 dr = \int_O^R G_3 dr + \int_O^R G_5 dr$$

where $G_5 = \rho g 2\pi r \dfrac{w^2}{2}$.

We now define

$$G_6 = G_2 - G_3 - G_5 = \eta P_{arc} 2\pi r w - \sigma 2\pi r \left[1 + \left(\frac{dw}{dr}\right)^2 \right]^{1/2} + \sigma 2\pi r - \rho g 2\pi r \frac{w^2}{2}$$

where $\int_O^R G_6 dr$ is the difference of work

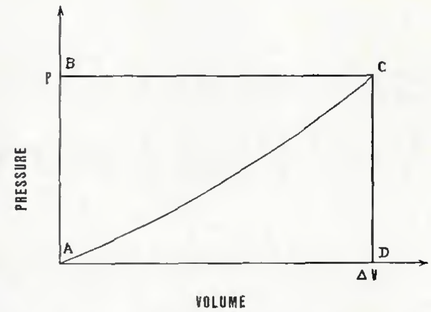

Fig. 3—Reversible and irreversible PΔV work. Reversible work is performed along path AC and irreversible work is performed along path ABC

performed by the arc force and the total system energy which is the summation of potential energy and surface energy.

If one applies the Euler-Lagrangian criterion (Ref. 12),

$$\frac{\partial}{\partial w}(F + \lambda_1 G_1 + \lambda_2 G_6) - \frac{\partial}{\partial r}\frac{\partial}{\partial (dw/dr)}(F + \lambda_1 G_1 + \lambda_2 G_6) = 0$$

where λ_1 and λ_2 are Lagrange multipliers; one has a function which must be minimized subject to the two constraints noted previously.

After manipulation, the result of the Euler-Lagrangian criterion is

$$\frac{dt}{dr} = \frac{(1+t^2)^{1/2}}{\sigma r(1-\lambda_2)}\Big[\rho g r w + \lambda_2 r(\eta P_{arc} - \rho g w) + \lambda_1 r - (1-\lambda_2)(1+t^2)^{-1/2} \cdot \left(\sigma t + r t \frac{d\sigma}{dr} - \sigma r \frac{t^2}{1+t^2}\right)\Big] \qquad (4)$$

if one sets

$$t = \frac{dw}{dr}. \qquad (5)$$

There are two boundary conditions

$t = 0$ at $r = 0$

due to symmetry about the centerline of the weld pool and

$w = 0$ at $r = R$

since the liquid must be in contact with the solid surface.

A computer program was developed to evaluate λ_1 and λ_2. After evaluating λ_1 and λ_2 together with suitable boundary conditions and constraints, equations (4) and (5) are then solved simultaneously by the Runge-Kutta method (Ref. 13).

Parametric Analysis of the Model

In this model, there are five parameters which may be related to the welding process. These are:

1. The density of the molten metal, ρ.
2. The surface energy of the molten metal, σ.
3. The half width of the weld pool, R.
4. The arc pressure, P_{arc}.
5. The efficiency of work conversion, η.

The shape of the liquid-solid boundary is not included in this model. This is reasonable if movement of the gas-liquid boundary is small compared to the dimension of the weld pool. It may be argued from hydrostatics that the shape of the solid-liquid boundary will not influ-

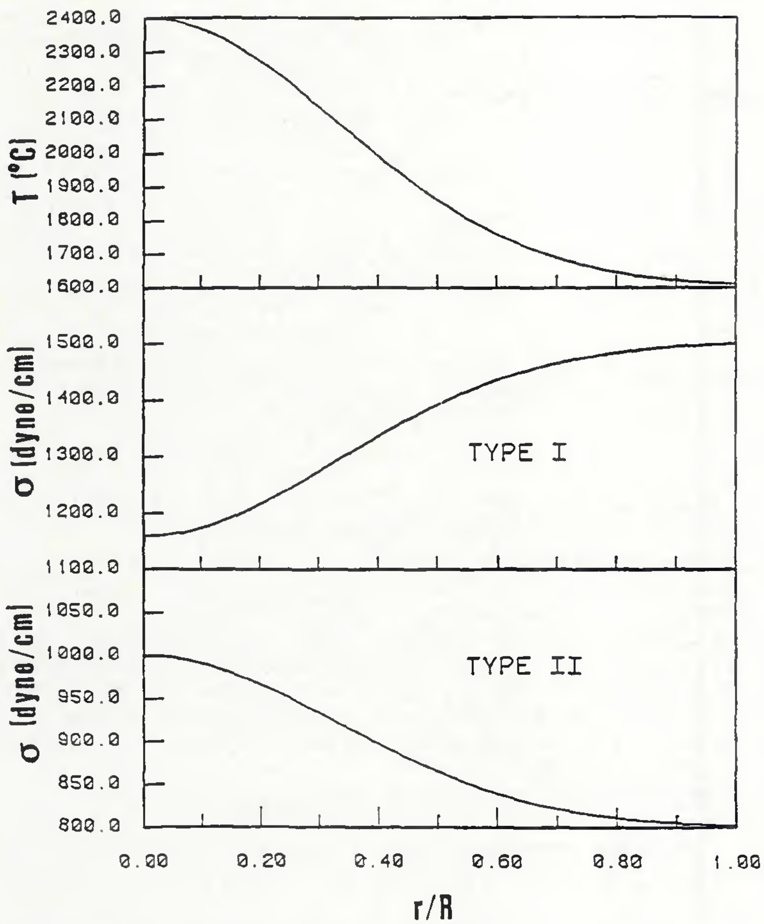

Fig. 4 — Assumed surface temperature and surface tension distribution of weld pool vs. reduced weld pool radius. Type I surface tension is believed to correspond to a steel without surface active elements while Type II surface tension is believed to represent a steel with surface active elements

ence the result, provided the gas-liquid boundary does not impinge upon the solid-liquid boundary.

Steel and aluminum are chosen in this model with densities equal to 7.84 g/cm^3 and 2.7 g/cm^3, respectively. For the distribution of surface energy of the molten pool, it is assumed that the temperature distribution on the top surface of the molten pool is as shown in Fig. 4A. The corresponding surface tension distributions are shown in Figs. 4B and 4C. Figure 4B is for pure iron, while Fig. 4C is for metal with high concentrations of surface active elements, *e.g.*, sulfur and oxygen (Ref. 14).

The magnitude of these temperature and surface tension distributions are not appropriate for aluminum; however, the main purpose of choosing these distributions is to investigate the effect of surface tension on surface depression of a molten pool. Other results could be calculated for aluminum if accurate surface tension values were available. The half width of the weld pool is assumed to range from 0.5 to 1 cm (0.2 to 0.39 in.).

The arc pressure is taken from literature (Ref. 2) as shown in Fig. 5, using the arc pressure measured at 300 A. With higher currents, simple multiplication of the arc pressure data from the 300 A curve is assumed. While this does not represent a physical reality, it may be sufficient to study the influence of arc pressure on surface depression of the weld pool.

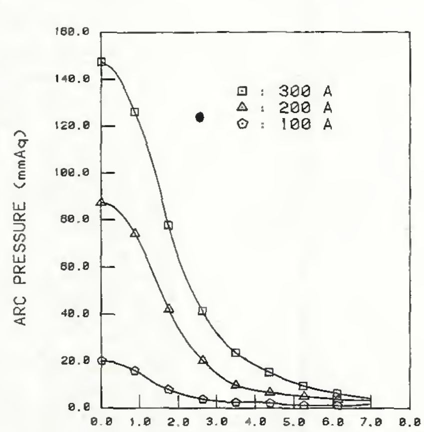

Fig. 5 — Arc pressure distribution taken from literature (Ref. 2). Polarity — DCEN; electrode — 4.0 mm (0.16 in.) diameter thoriated tungsten (90 deg); shielding gas — Ar; arc length — 5 mm (0.197 in.)

Two values, 50 and 100%, are used to account for the efficiency of conversion of work done by the arc force to the change of surface energy and potential energy of the weld pool. The value of 100% corresponds to path ABC of Fig. 3, while the value of 50% corresponds approximately to path AC.

Results

The results of this model are shown in Figs. 6 to 11. A more complete set of tabulated results are listed in Table 1. The maximum depth of surface depression of the molten pool varies from 0.49 to 38.178 mm (0.019 to 1.504 in.); however, for reasonable pressures exerted by a 300 A arc, the maximum value is less than 1.3 mm (0.05 in.) for a 1 cm (0.39 in.) wide liquid steel pool. This is much less than the experimentally observed value of over 4 mm (0.16 in.) — Fig. 1.

Density of Molten Metal

When the density of molten metal increases, the surface depression depth is reduced as shown in Figs. 6 to 11. The effect of density becomes more prominent when the top surface of the weld pool becomes deeper. In Fig. 6, the maximum depth of surface depression for steel is 0.49 mm (0.019 in.) and for aluminum the maximum depth of surface depression is 0.642 mm (0.025 in.). Hence, reducing the density by nearly a factor of three increases the depression by only 30%. However, at higher arc pressures, as seen in Fig. 10, low density liquid has a maximum depth 160% larger than that of the heavy liquid.

Surface Tension

The effect of surface tension on the depth of surface depression of the weld pool is shown in Figs. 6 to 8. For the assumed surface tension distributions (types I and II as shown in Figs. 4B and 4C), the effect of surface tension on the shape of surface depression is not very important in both the low and the high surface depression ranges. The maximum surface depression depth is found to vary only 20% for the high density liquid and 40% for the low density liquid due to these different surface tension distributions.

Width of Weld Pool

The effect of weld pool width can be seen in Fig. 9 or by comparing Figs. 6 and 7. When the width of the weld pool increases, the surface depression depth also increases. As can be seen in Fig. 9,

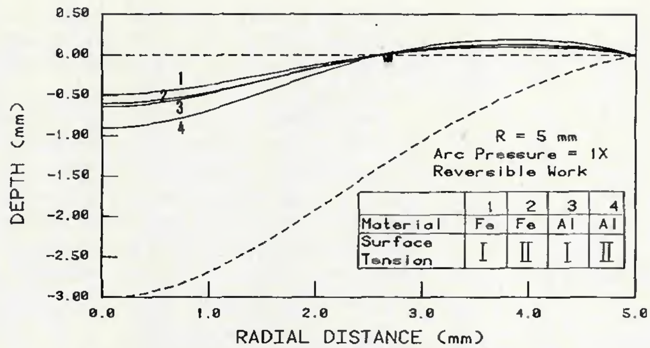

Fig. 6—Half surface depression curve at 300 A arc pressure assuming reversible work and a 1.0 cm (0.39 in.) wide weld pool. The dotted curve represents an approximate liquid-solid boundary

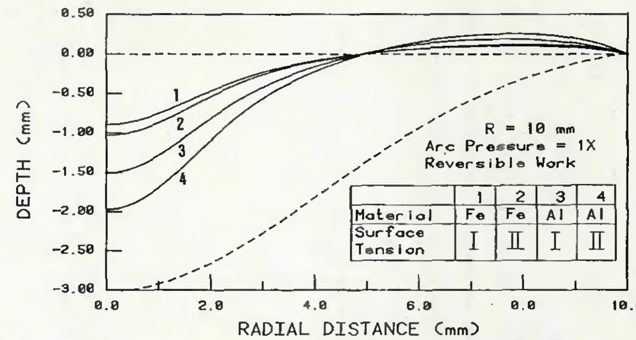

Fig. 7—Half surface depression curve at 300 A arc pressure assuming reversible work and a 2.0 cm (0.79 in.) wide weld pool. The dotted curve represents an approximate liquid-solid boundary

when the surface depression depth is small, the maximum depth increases only 80% when the weld pool width increases from 10 to 20 mm (0.39 to 0.79 in.). However, when the surface depression depth is large, the maximum depth increases 140% when the weld pool width increases from 10 to 20 mm (0.39 to 0.79 in.).

Arc Pressure

The arc pressure at 300 A causes a shallow depression (less than 2 mm, *i.e.*, 0.078 in.). However, when the arc pressure is very high, as shown in Figs. 10 and 11, the surface depression becomes very large. This may imply that at higher currents, the depth of surface depression is dominated by the strong arc pressure.

It should be noted that if the pressure distribution remains fixed in size, but increases parabolically with current, the pressures of 2, 4 and 6 times the measured pressure at 300 A would correspond to currents of 425, 600 and 735 A, respectively. If, on the other hand, the maximum pressure scales linearly with current, as has been confirmed in our laboratory (Ref. 15), these pressures would correspond to 600, 1200 and 1800 A, respectively.

Work Conversion

The calculated depth of surface depression of irreversible work conversion is about two times larger than that of reversible work conversion, as shown in Figs. 9 and 11, which is not surprising.

Discussion

One of the more obvious criticisms of this model is the lack of a positive basis

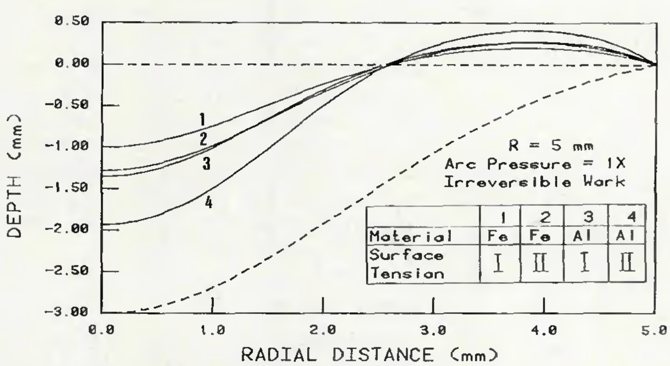

Fig. 8—Half surface depression curve at 300 A arc pressure assuming irreversible work. Compare with Fig. 6. The dotted curve represents an approximate liquid-solid boundary

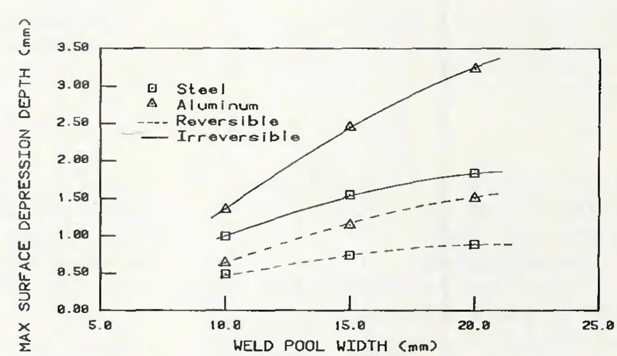

Fig. 9—Maximum surface depression depth vs. weld pool width for different materials and types of work conversion

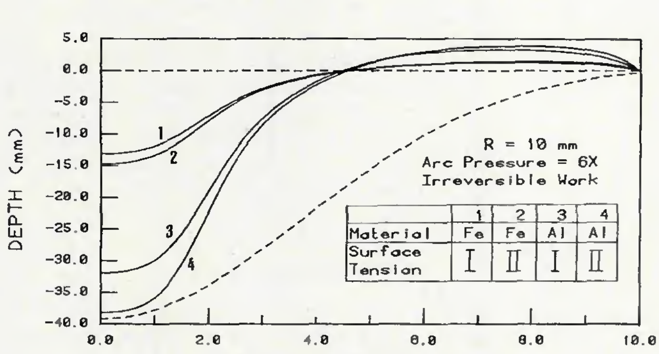

Fig. 10—Half surface depression curve at extreme arc pressure. The dotted curve represents an approximate liquid-solid boundary

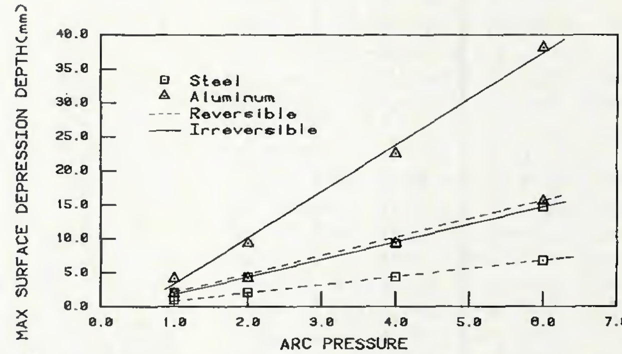

Fig. 11—Maximum surface depression depth versus arc pressure for different materials and types of work conversion. The numbers on the abscissa represent the multiplication factor of the arc pressure of the 300 A current in Fig. 5

Table 1—Calculated Maximum Depth of Surface Depression

Material	Half width, mm[a]	Arc pressure[b]	Surface tension	Work conversion	Max. depth of surface depression, mm[a]
Steel	5	1X	Type I	Rev.	0.490
Steel	5	1X	Type II	Rev.	0.600
Aluminum	5	1X	Type I	Rev.	0.642
Aluminum	5	1X	Type II	Rev.	0.903
Steel	10	1X	Type I	Rev.	0.893
Steel	10	1X	Type II	Rev.	1.029
Aluminum	10	1X	Type I	Rev.	1.511
Aluminum	10	1X	Type II	Rev.	1.975
Steel	5	1X	Type I	Irrev.	1.000
Steel	5	1X	Type II	Irrev.	1.282
Aluminum	5	1X	Type I	Irrev.	1.354
Aluminum	5	1X	Type II	Irrev.	1.938
Steel	10	1X	Type I	Irrev.	1.846
Steel	10	1X	Type II	Irrev.	2.127
Aluminum	10	1X	Type I	Irrev.	3.237
Aluminum	10	1X	Type II	Irrev.	4.210
Steel	5	2X	Type I	Rev.	1.000
Steel	5	2X	Type II	Rev.	1.279
Aluminum	5	2X	Type I	Rev.	1.354
Aluminum	5	2X	Type II	Rev.	1.938
Steel	10	2X	Type I	Rev.	1.857
Steel	10	2X	Type II	Rev.	2.132
Aluminum	10	2X	Type I	Rev.	3.235
Aluminum	10	2X	Type II	Rev.	4.212
Steel	10	6X	Type I	Irrev.	13.162
Steel	10	6X	Type II	Irrev.	14.731
Aluminum	10	6X	Type I	Irrev.	31.939
Aluminum	10	6X	Type II	Irrev.	38.178
Steel	5	2X	Type I	Irrev.	2.150
Steel	5	2X	Type II	Irrev.	2.712
Aluminum	5	2X	Type I	Irrev.	3.069
Aluminum	5	2X	Type II	Irrev.	4.650
Steel	10	6X	Type II	Rev.	6.821
Aluminum	10	6X	Type II	Rev.	15.572
Aluminum	5	4X	Type II	Rev.	4.641
Aluminum	10	4X	Type II	Rev.	9.372
Steel	7.5	1X	Type I.	Rev.	0.741
Aluminum	7.5	1X	Type I	Rev.	1.142

(a)25.4 mm = 1 in.
(b)This represents multiplication of the 300 A arc pressure data given in Fig. 5.

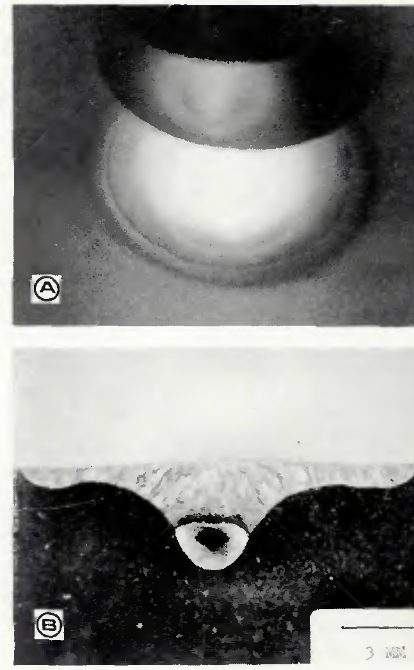

Fig. 12—Surface depression at 300 A of a stationary arc weld on Type 304 stainless steel: A—top surface during welding showing deep narrow depression; B—cross section of same weld. Note the porosity at the bottom of this finger indicating that the depression penetrated to the very bottom of the weld

for selection of the work conversion efficiency, η. Although no direct rationale can be given for choosing either path ABC or path AC of Fig. 3, it is felt that path AC is more realistic. This is perhaps easiest to explain if one considers not the total depression from an initially flat metal surface to a fully depressed state; but rather, one might consider a small differential depression from an already depressed surface, due to minor arc pressure fluctuations. Such a restoration to a new equilibrium must follow path AC more closely than path ABC.

In addition, by viewing this system as a dynamic equilibrium where small changes in the arc force produce corresponding changes in the equilibrium surface shape, one can easily understand why other forms of energy (*e.g.*, thermal energy) need not be considered to contribute to the formation of new surface area. Even if thermal energy were to create new surface area, the system must finally consume such new area as it is only the arc force which balances the surface tension forces of the curved boundary. At final equilibrium, thermal energy cannot be considered to contribute to the balance of the arc force. Only other forces such as surface tension and hydrostatic forces can balance the arc force.

Finally, even if rather generous increases in arc force are postulated, it is seen that the experimentally observed surface depressions at 300 A cannot easily be explained by the arc force, no matter what the work conversion efficiency is assumed to be.

Experimentally, it has been observed that the surface depression at currents below 200 A is negligible. However, when current increases to about 300 A, a deep surface depression is found, as shown in Fig. 12. The maximum depth of surface depression is about 4.5 mm (0.18 in.) for stainless steel weld pools. From the model of the arc pressure, it is seen that the arc pressure cannot explain the deep surface depression at 300 A current, since the maximum depth of surface depression which was calculated for steel is 1.28 mm (0.050 in.). This is much smaller than the actual depth of surface depression which is experimentally found to be 4.5 mm (0.18 in.). Thus, some other mechanism must be responsible for the deep surface depression at these higher currents.

A simplified vortex model is proposed in this work to account for the deep surface depression at high currents. In this model, a compound vortex consisting of a forced vortex in the central part of the liquid pool with a free vortex surrounding the forced vortex is assumed.* This is shown schematically in Fig. 13. The result of the compound vortex model is shown in Fig. 14, assuming several angular velocities for the forced vortex. It can be seen that the depth of surface depression caused by the compound vortex can be close to the actual depth of the surface depression at high currents for angular velocities between 20 and 30 rad/s. Such circumferential flow can be seen in high

**A forced vortex is a region where the angular velocity ω_f is a constant. A free vortex is one that has constant angular momentum, i.e., $v_\theta = K/r$, where K is the vortex constant and θ is the azimuthal direction of cylindrical coordinates. The compound vortex matches a free vortex near the solid boundary with a forced vortex in the center of the weld pool.*

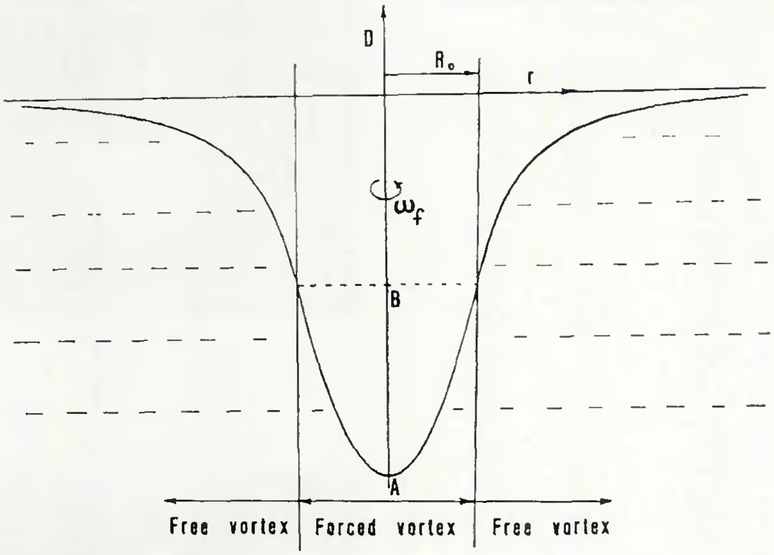

Fig. 13 — Structure of the compound vortex. Assuming no transition region between the forced and free vortex

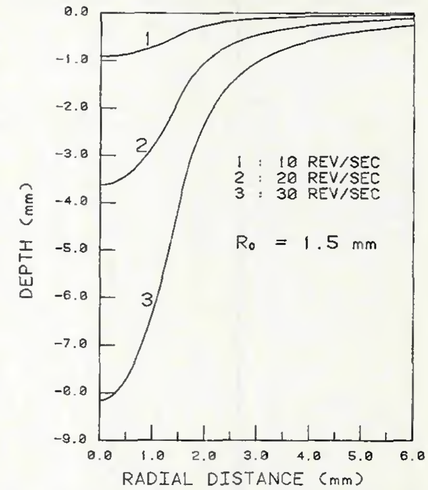

Fig. 14 — Depth induced by a compound vortex with a forced vortex region of 1.5 mm (0.06 in.) radius

speed movies of weld pools, which have oxide particles floating on the surface.

Flow, as that described above, may come from the toroidal flow on the plane parallel to the arc axis. Millere (Ref. 16) found that in electrically driven toroidal flow, a circumferential rotational motion on the plane normal to the arc axis is produced and increases with the intensity of electrovortex (toroidal flow) on the plane parallel to the arc axis. Therefore, part of the kinetic energy of toroidal flow on the plane parallel to the arc axis is transferred to circumferential motion, inducing flow on the plane normal to the arc axis.

It will be appreciated from Millere's work that such circumferential flow will not be strong if the system has perfect cylindrical symmetry. In real systems without perfect symmetry, the axial toroidal flow vector will be displaced from the center line resulting in a circumferential velocity component which causes a circumferential precession of the toroidal flow into a helical shape. It should be noted that the maximum circumferential velocities assumed in Fig. 14 are less than one third of the velocities noted by Heiple and Roper (Ref. 17) using high speed cinematography; hence, these assumed rotational speeds are thought to be consistent with observed motion in actual weld pools.

As a result of this study, three current ranges may be proposed to explain surface depression of weld pools. At low currents (below about 200 A), the weld pool depression is shallow and does not significantly influence the shape of the weld pool. At higher currents (from about 300 to 500 A), the surface depression greatly influences the weld pool geometry. A circumferential vortex flow may be responsible for the formation of this surface depression and the presence of the 'finger' penetration seen in gas tungsten arc spot welds, GMAW and SAW beads. At even higher currents (above about 500 A)*, the arc pressure is strong enough that it may explain some of the deep surface depression which, in turn, influences the weld pool geometry. The three current ranges proposed in this model are consistent with the results of Chihoski (Ref. 18) who found four distinct current ranges for the depth of penetration in aluminum welds. In his study, the penetration shows a very slow increase with current in the 100-200 A range, followed by a steep increase with current in the 200-300 A range. The 300-400 A range shows almost no response of current to penetration, but in the 450-600 A range, penetration begins to increase moderately with current.

Chihoski's 100-200 A range corresponds to the regime where surface depression is controlled by arc force and is not significant. The 200-300 A range corresponds to the transition from little surface depression to formation of a full vortex, while the 300-400 A range corresponds to bottoming out of the vortex depression at the solid boundary. In such a case, the current from the arc, or the heat, follows paths normal to the isopotential lines in the plasma and, hence, is concentrated at the top edges of the liquid vortex.

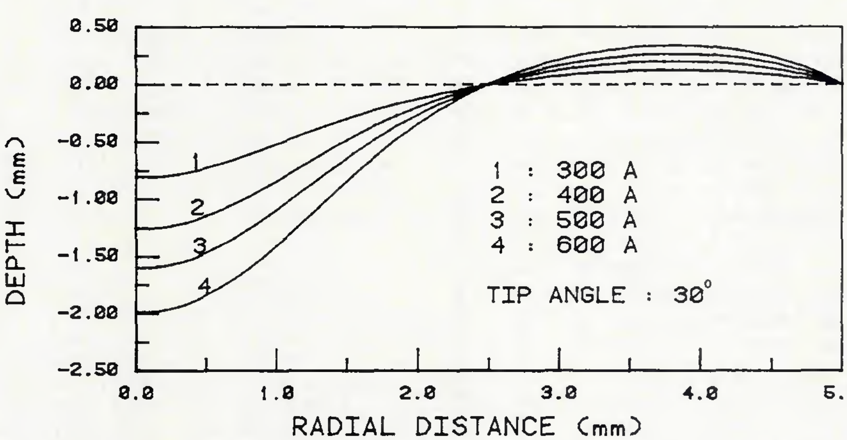

Fig. 15 — Half surface depression curve at different currents assuming reversible work. These surface depression curves are caused by the arc pressure measured in our laboratory

**More recent work by Lin and Eagar (Ref. 15) has shown that the depth of surface depression caused by the measured arc pressure at 600 A still cannot explain the deep crater of the weld pool found at even lower currents. Figure 15 shows the depth of the surface depression caused by the arc pressure measured in our laboratory.*

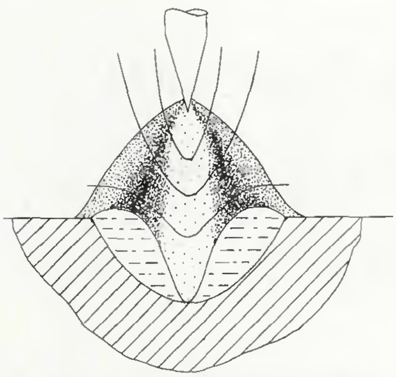

Fig. 16 — Schematic representation of the equipotential lines and the current density distribution when a deep crater forms. Note that the equipotential lines around a deep depression suggest that the arc current (and hence the thermal energy) is distributed to the side walls of the pool and very little current (i.e., heat) reaches the bottom of the depression, as is depicted by the shaded region. Increased penetration due to the vortex formation is thus effectively stopped

As such, direct arc heat does not reach the bottom of the vortex, as shown in Fig. 16. Hence, no further melting occurs at the bottom of the depression and no further penetration results. Above 450 A, the arc pressure becomes significant and, together with the vortex, deepens the depression as the current is increased.

Although the analytical arc force model presented here applies only to partial joint penetration welds,* it is believed that the vortex model is applicable to both complete and partial joint penetration beads. However, more study of the strength and mechanism of vortex formation is needed to confirm this hypothesis. Finally, it should be noted that if arc force were in fact the dominant cause of surface depression in welding, the depression would change markedly with changes in liquid density.

When a vortex is considered the cause of surface depression, there is no dependence of depression on density. The fact that finger penetrations in aluminum and steel are of nearly equal depth is considered supportive of the vortex model. In addition, the experimental shape of finger penetration, as seen in Fig. 12B, is thought to be more consistent with a vortex model than an arc force model.

For an analysis of arc force on full penetration welds, see Friedman (Ref. 9).

Conclusion

The depth of surface depression caused by the arc pressure distribution has been calculated using calculus of variations with suitable constraints. The results show that arc pressure only influences weld pool geometry at currents in excess of 500 A. At intermediate currents, the shape of the pool may be influenced markedly by circumferential convection. This flow may be responsible for the characteristic finger penetration of many weld pools. At even higher currents, arc force may become important and may have a significant influence on weld pool geometry.

Acknowledgments

The authors are grateful for support of this work by the Office of Naval Research under Contract N00014-C-80-0384. They also wish to thank the reviewers of this paper for their great care and many useful suggestions.

References

1. Selyanenkov, V. N., Stepanov, V. V., and Saifiev, R. Z. 1980. The dependence of the pressure of the welding arc on the parameters of tungsten electrodes. *Welding Production* 27(5): 6-8.
2. Unpublished technical support. 1980. Osaka Transformer Co., Osaka, Japan.
3. Shchetinina, V. I., *et al.* 1981. The dependence of the distribution of arc pressure on welding speed. *Welding Production* 28(4): 1-2.
4. Mazel', A. G., Yatsenko, V. P., and Rogova, E. M. 1977. On the force effect of the arc plasma flow on the weld pool. *Welding Production* 24(7): 5-8.
5. Stepanov, V. V., *et al.* 1977. Distribution of pressure in the plasma arc, and effects of the rate of flow of plasma-forming gas on weld quality. *Auto. Weld.* 30(6): 5-7.
6. Yamauchi, N., *et al.* 1980. Development and application of high TIG process-SHOLTA welding process. *Proceedings of International Conference on Welding Research in the 1980's*, Osaka, October, 1980, pp. 25-30.
7. Savage, W. F., Nippes, E. F. and Agusa, K. 1979. Effect of arc force on defect formation in GTA welding. *Welding Journal* 58(7): 212-s to 224-s.
8. Ishizaki, K. 1980. A new approach to the mechanism of penetration. *Weld Pool Chemistry and Metallurgy*, pp. 65-70. The Welding Institute International Conference, London, April, 1980.
9. Friedman, E. 1978. Analysis of weld puddle distortion and its effect on penetration. *Welding Journal* 56(6): 161-s and 166-s.
10. Lin, M. L., and Eagar, T. W. 1983. Influence of surface depression and convection on arc weld pool geometry. *Transport Phenomena in Materials Processing*, ASME PED-Vol. 10, November 1983, pp. 63-69.
11. Burleigh, T. D., and Eagar, T. W. 1983. Measurements of the force exerted by a welding arc. *Met. Trans.* 14A(6): 1223-1224.
12. Ketter, R. L., and Prawel, S. P., Jr. 1969. *Modern methods of engineering computation.* New York: McGraw-Hill.
13. Milne, W. E. 1962. *Numerical solution of differential equation.* New York: John Wiley & Sons.
14. Keene, B. J., *et al.* 1982. Effects of interaction between surface active elements on the surface tension of iron. *Canadian Metallurgical Quarterly* 21(4): 393-403.
15. Lin, M. L., and Eagar, T. W. Unpublished work.
16. Millere, R. P., *et al.* 1980. Effect of a longitudinal magnetic field on electrically driven rotational flow in a cylindrical vessel. *Magnetohydrodynamics* 16(1): 66-69.
17. Heiple, C. R., Roper, J. R., Stagner, R. T., and Aden, R. J. 1983. Surface active element effects on the shape of GTA, laser, and electron beam welds. *Welding Journal* 62(3): 72-s to 77-s.
18. Chihoski, R. A. 1970. The rationing of power between the gas tungsten arc and electrode. *Welding Journal* 49(2): 69-s to 82-s.

Appendix

Referring to Fig. 13, the depth produced by a compound vortex may be estimated as follows:

In the forced vortex region ($r \leq R_0$), the angular velocity is constant, and

$$D_1 = \frac{\omega_f^2 r^2}{2g}$$

with the origin referred to point A in Fig. 13.

In the free vortex region ($r > R_0$), the angular momentum is constant, and:

$$D_2 = \frac{\omega_f^2 R_0^4}{2g}\left(\frac{1}{R_0^2} - \frac{1}{r^2}\right)$$

with the origin referred to point B in Fig. 13. The total depression $D = D_1 + D_2$.

List of Symbols

- T — temperature on the surface of weld pool (°C)
- J — total system energy(erg)
- σ — surface energy(erg/cm^2)
- ρ — density of liquid metal(g/cm^3)
- g — gravitational acceleration(cm/s^2)
- h — ordinate of solid-liquid boundary(cm)
- w — ordinate of liquid-gas boundary(cm)
- r — radial coordinate of weld pool(cm)
- H — maximum depth of liquid pool(cm)
- R — radius of the top surface of liquid pool(cm)
- η — percentage of work conversion(%)
- D — depth of liquid pool produced by a compound vortex(cm)
- R_0 — radius of forced vortex region(cm)
- ω_f — angular velocity of rotational motion in forced vortex region(rad/s)